Chirality Versus Symmetry: Electron's Spin Selectivity in Non-Polar Chiral Lead-Bromide Perovskites

Alexandre Abhervé, Nicolas Mercier, Anil Kumar, Tapan Kumar Das, Jacky Even, Claudine Katan, Mikaël Kepenekian

ADVANCED MATERIALS
www.advmat.de

Chirality Versus Symmetry: Electron's Spin Selectivity in Nonpolar Chiral Lead–Bromide Perovskites

Alexandre Abhervé, Nicolas Mercier, Anil Kumar, Tapan Kumar Das, Jacky Even, Claudine Katan, and Mikaël Kepenekian**

In the last decade, chirality-induced spin selectivity (CISS), the spin-selective electron transport through chiral molecules, has been described in a large range of materials, from insulators to superconductors. Because more experimental studies are desired for the theoretical understanding of the CISS effect, chiral metal-halide semiconductors may contribute to the field thanks to their chiroptical and spintronic properties. In this regard, this work uses new chiral organic cations *S*-HP1A and *R*-HP1A (HP1A = 2-hydroxy-propyl-1-ammonium) to prepare 2D chiral halide perovskites (HPs) which crystallize in the enantiomorphic space groups $P4_32_12$ and $P4_12_12$, respectively. The fourfold symmetry induces antiferroelectricity along the stacking axis which, combined to incomplete Rashba-like splitting in each individual 2D polar layer, results in rare spin textures in the band structure. As revealed by magnetic conductive-probe atomic force microscopy (AFM) measurements, these materials show CISS effect with partial spin polarization (SP; ±40–45%). This incomplete effect is efficient enough to drive a chiro-spintronic device as demonstrated by the fabrication of spin valve devices with magnetoresistance (MR) responses up to 250 K. Therefore, these stable lead–bromide HP materials not only represent interesting candidates for spintronic applications but also reveal the importance of polar symmetry-breaking topology for spin selectivity.

1. Introduction

The emergent field of chiro-spintronics is based on using chiral molecules as a substitute for ferromagnetic (FM) materials thanks to the spin-specific interaction between electrons and chiral molecules, a phenomenon called CISS, "chirality-induced spin selectivity".[1] Hence, chiro-spintronic devices can control both electronic and spin properties without application of external magnetic field or excitation by circularly polarized light (CPL). The current challenge is to reveal the microscopic origins of CISS, therefore, a combined experimental and theoretical study on a model system is strongly desired.[2] In this context, two-dimensional (2D) or one-dimensional (1D) halide perovskites (HPs) are interesting compounds since they recently showed promising chiroptical and chiroptoelectronic properties.[3] Based on theoretical investigation, it has been suggested that circular dichroism (CD) may also arise in nonchiral inorganic HP compounds through the interplay of excitonic and Rashba effects.[4] So far, intrinsic chirality has been reported for low-dimensional HP with chiral organic cations inserted in the inorganic metal-halide network. This strategy provides opportunities to tune the chiral performances by chemical engineering. For organic materials, it has been demonstrated that increasing length[5] or helical pitch[6] of the organic molecule results in an increase of the spin selectivity. Hybrid HP compounds have been reported to favor spin transport related to the CISS effect.[7–9] They revealed great potential for optoelectronic applications, for example as nonlinear optical materials[10] or CPL emitters,[11] and chiro-spintronic devices such as CPL detectors[12] or spin-LEDs.[13] Improving stability and

A. Abhervé, N. Mercier
MOLTECH-Anjou
UMR 6200
CNRS
UNIV Angers
2 bd Lavoisier, ANGERS, Cedex 49045, France
E-mail: alexandre.abherve@univ-angers.fr

The ORCID identification number(s) for the author(s) of this article can be found under https://doi.org/10.1002/adma.202305784

DOI: 10.1002/adma.202305784

A. Kumar, T. K. Das
Department of Chemical and Biological Physics
Weizmann Institute of Science
Rehovot 76100, Israel

J. Even
Univ Rennes
INSA Rennes
CNRS
Institut FOTON – UMR 6082, Rennes F-35000, France

C. Katan, M. Kepenekian
Univ Rennes
ENSCR
CNRS
ISCR – UMR 6226, Rennes F-35000, France
E-mail: mikael.kepenekian@univ-rennes1.fr

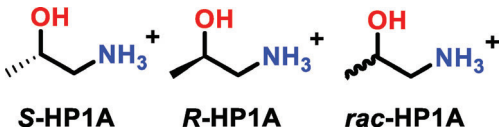

Scheme 1. Structures of the chiral cations.

performances is crucial for practical applications of optoelectronic and spintronic devices. In this regard, one must consider the chemical design of the chiral perovskite. In particular, replacement of iodide with bromide anions can improve the stability of the active material and long-term durability of the device.[14] Furthermore, local asymmetry in the 2D inorganic layers has more often been reported for lead–bromide compounds than for lead–iodide.[15]

Regarding the physical origin of the observed chiral effect either at the material level or in a device configuration, a number of questions are still open. In chiral HPs, it was envisaged that a strong chirality would require the combination of high order symmetry operations (≥3) with spatial inversion symmetry breaking.[16] However, chirality in HPs is mostly associated with the presence of only twofold rotation/screw axes in the crystal structures. The presence of such polar axes is expected to induce various Rashba-like effects in the electronic band structures associated with the perovskite backbone, eventually with an in-plane polar axis leading to partial splitting of the spin states and incomplete spin textures.[17,18] The interplay between the Rashba effect and chirality has been inferred in many practical examples of HPs exhibiting chiral effects.[19] However, in a more classical view, chirality should be related to a helicity in the crystallographic structure. As described in the theoretical model of Yu on chirality-induced spin-orbit coupling (SOC) in HPs,[20] several parameters, such as the distances between inorganic networks and the helical arrangement of organic cations, should affect the effective SOC coupling and out-of-plane electron transport in chiral HPs. Higher-order symmetry operations are then required to experimentally and theoretically evaluate the impact of helical potential on the target physical properties of HPs. Electrons moving along a high order axis may experience an extra SOC corresponding to the geometric SOC in a helix.[20] In addition, among the 65 types of Sohncke space groups in which chiral molecules can crystallize, 22 (11 enantiomorphic pairs) are intrinsically chiral. Up to date, only one example of HP structures crystallizing in a pair of chiral space groups has been reported by Miyasaka et al. They revealed the influence of chirality for the circular photogalvanic effect in lead–iodide compounds.[21] For this nonpolar bulk structure, the observed effect was ascribed to a hypothetical spin-texture different from that expected for a Rashba effect in a polar system.

Here we report two lead–bromide enantiomers of formula $(S\text{-HP1A})_2PbBr_4$ and $(R\text{-HP1A})_2PbBr_4$ (*S*/*R*-HP1A = (*S*/*R*)−2-hydroxy-propyl-1-ammonium, **Scheme 1**), crystallizing in the enantiomorphic $P4_32_12$ and $P4_12_12$ chiral space group pair. The structural characterization and in-depth theoretical investigation of their band structure and spin texture, together with CISS measurements and spin-valve devices, revealed the impact of symmetry elements in this family of chiral HPs. Our interpretation regarding the influence of the electronic structure and spin textures differs from that proposed by Miyasaka et al. Rationalization of the present results along with those reported earlier for other nonpolar systems is obtained based on the antiferroelectricity and alternating incomplete Rashba-like splittings of the successive perovskite layers piled up along the stacking axis.

2. Results and Discussion

Single crystals of $(S\text{-HP1A})_2PbBr_4$, $(R\text{-HP1A})_2PbBr_4$ and $(rac\text{-HP1A})_2PbBr_4$ were obtained using the liquid/vapor diffusion technique. After slow diffusion of ethyl acetate into a hydrobromic acid solution of $PbBr_2$ and pure *S*, *R* or racemic 1-amino-2-propanol, millimeter-size colorless platelets could be obtained (Figure S1, Supporting Information). Single-crystal X-ray diffraction measurements revealed that the structures made with the *S* and *R* enantiomers crystallize in the $P4_32_12$ and $P4_12_12$ nonpolar space groups, respectively, with one independent $PbBr_5$ unit and two independent cations in the asymmetric unit. On the other hand, with the racemic cation, the compound crystallized in the monoclinic system with $P2_1/c$ space group (Figure S2 and Table S1, Supporting Information). The structures belong to the Ruddlesden–Popper family of 2D HPs and present slight shifts between neighboring staggered inorganic layers (**Figure 1**). In the enantiomorphic compounds, the interlayer distance of 12.47 Å (i.e., a quarter of the *c* parameter value) is among the shortest in the family of lead or tin-based 2D chiral HPs reported to date, usually falling in the range 14.36–19.50 Å (Table S2, Supporting Information). Only one lead–iodide compound bearing a shorter interlayer distance of 11.54 Å could be afforded using the divalent cation *S*-4-NH_3-MBA.[15]

Pb–Br bond distances are in the range 2.927(3)–3.0763(13) Å in $(S\text{-HP1A})_2PbBr_4$ and 2.923(3)–3.0774(11) Å in $(R\text{-HP1A})_2PbBr_4$ (**Table 1**). In-plane distortions appear from the bond distance differences in the equatorial plane and large planar deviations of Pb–Br–Pb angles (144.5(2)–157.81(16)° in $(S\text{-HP1A})_2PbBr_4$, 144.74(18)–157.88(14)° in $(R\text{-HP1A})_2PbBr_4$). Due to the fourfold symmetry, the unit cells contain four 2D layers with different orientation (**Figure 2**). The $4_1/4_3$ screw axes induce a peculiar stacking since each layer turns 90° with its closest neighbor, leading to different orientation of the distortion. Indeed, wavy-like chains of Pb1-Br4-Pb1-Br4 with intermediate bond distances run along the [110] direction in layers 1 and 3 and along the [1–10] direction in layers 2 and 4 (Figure 2). In the perpendicular direction (i.e., [1–10] for layers 1 and 3, [110] for layers 2 and 4), an alternation of longest Pb1-Br3 and smallest Pb1-Br5 bonds is observed. In addition to bond lengths, a strong tilting between adjacent octahedra is highlighted by the three different equatorial Pb–Br–Pb bond angles (Table 1). The strong disparity between adjacent bond angles (Δ >13°) is expected to have a major influence on the strength of the spin-splitting, as recently demonstrated by Mitzi et al. for a series of 2D chiral HPs.[15] Finally, a small distortion appears from the two different bond distances with apical bromide ions, however the direction of the distortion alternates between adjacent octahedra, thus leading to the absence of polarity along the [001] direction. In the racemic compound, due to the low-order symmetry associated to the $P2_1/c$ space group, there is only one 2D layer in the unit cell (Figures S2–S4, Supporting Information). Very similar Pb–Br bond distances of 2.984(3)–3.0062(14) Å are observed and all Pb–Br–Pb angles have the same value of 153.38(7)° (Table S3, Supporting Information).

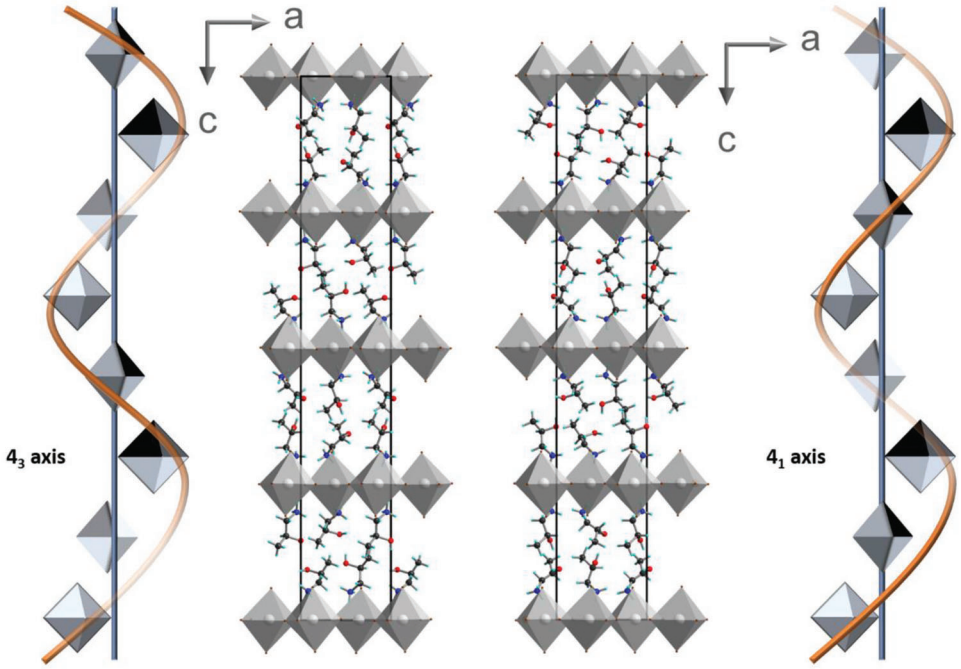

Figure 1. View of the crystal structures of $(S\text{-HP1A})_2PbBr_4$ and $(R\text{-HP1A})_2PbBr_4$ along the *c* axis with illustration of the 4_3 and 4_1 symmetry elements.

Overall, since the presence of screw axes results in helicity, one could expect that the 4_1 and 4_3 screw axes induce a strong helical potential that influences the spin polarization (SP) in the material. However, as illustrated in Figure 2, the 90° rotation between neighboring layers induces a change in the polarization direction. What are the real consequences of such crystal packing on the band dispersion and spin texture? The electronic structure of $(rac\text{-HP1A})_2PbBr_4$ and the pure-enantiomer-based $(S\text{-HP1A})_2PbBr_4$ have been probed by means of calculations based on density functional theory (DFT). The band structure of the racemic and enantiomer-based compounds presents similar features (**Figure 3** and Figure S6, Supporting Information), among which a computed band gap of 1.87 eV, and a 2D-like behavior characterized by a strong in-plane dispersion and a weak dispersion (lesser than 5 meV) in the stacking direction. In both cases, the top valence bands are dominated by Br-*p* and Pb-*s* states, while the lowest conduction states are mostly composed of Pb-*p* and Br-*s* states (Figure S7, Supporting Information). A striking contrast appears when going from $(rac\text{-HP1A})_2PbBr_4$ to $(S\text{-HP1A})_2PbBr_4$ and $(R\text{-HP1A})_2PbBr_4$ with a splitting of the top valence bands and bottom conduction bands away from the high-symmetry Γ point of the Brillouin zone. The splitting of the spin states around the Γ point, share similarities with Rashba–Dresselhaus spin splitting commonly observed in polar structures with heavy atoms marked by strong SOC effects. However, in the case of a 2D system the splitting of bands in both in-plane directions would then correspond to a polar axis along the stacking axis leading to a complete effect (Figure S8, Supporting Information).[17] In the nonpolar chiral structures here-presented, such a result is therefore unexpected at first glance.

Table 1. Selected bond distances and angles.

Atoms	$(S\text{-HP1A})_2PbBr_4$	$(R\text{-HP1A})_2PbBr_4$
	Bond distances [Å]	
Pb1–Br1	3.044(3)	3.036(3)
Pb1–Br2	2.927(3)	2.923(3)
Pb1–Br3	3.0763(13)	3.0774(11)
Pb1–Br4	3.012(3)	3.013(3)
Pb1–Br4	3.016(3)	3.024(3)
Pb1–Br5	2.968(2)	2.9710(17)
	Angles [°]	
Pb1–Br3–Pb1	157.81(16)	157.88(14)
Pb1–Br4–Pb1	152.01(14)	151.80(12)
Pb1–Br5–Pb1	144.5(2)	144.74(18)

A better understanding of the band structure is provided by considering each one of the four 2D inorganic layers independently. Each individual layer is intrinsically chiral due to both 2 and 2_1 axes resulting in the in-plane distortion and leading to a *C*2 point group symmetry. The in-plane band structure is described in the two directions perpendicular to the *c* axis (**Figure 4**a). In $(S\text{-HP1A})_2PbBr_4$, layers 1 and 3 present a conduction and valence band splitting along Γ→M' direction of the Brillouin zone but not along Γ→M direction. Such a feature is typical of an incomplete Rashba splitting observed when the polar axis is perpendicular to the stacking direction (Figure S8, Supporting Information),[17] thus confirming the presence in layers 1 and 3 of a polar axis along the [110] direction, i.e., along the direction of the Pb1-Br4-Pb1-Br4 bonds. The exact opposite is found for layers 2 and 4 since their orientation is shifted by 90° relative to layers 1 and 3 due to the $4_1/4_3$ symmetry. Therefore, the splitting is only observed along Γ→M direction, while the polar axis

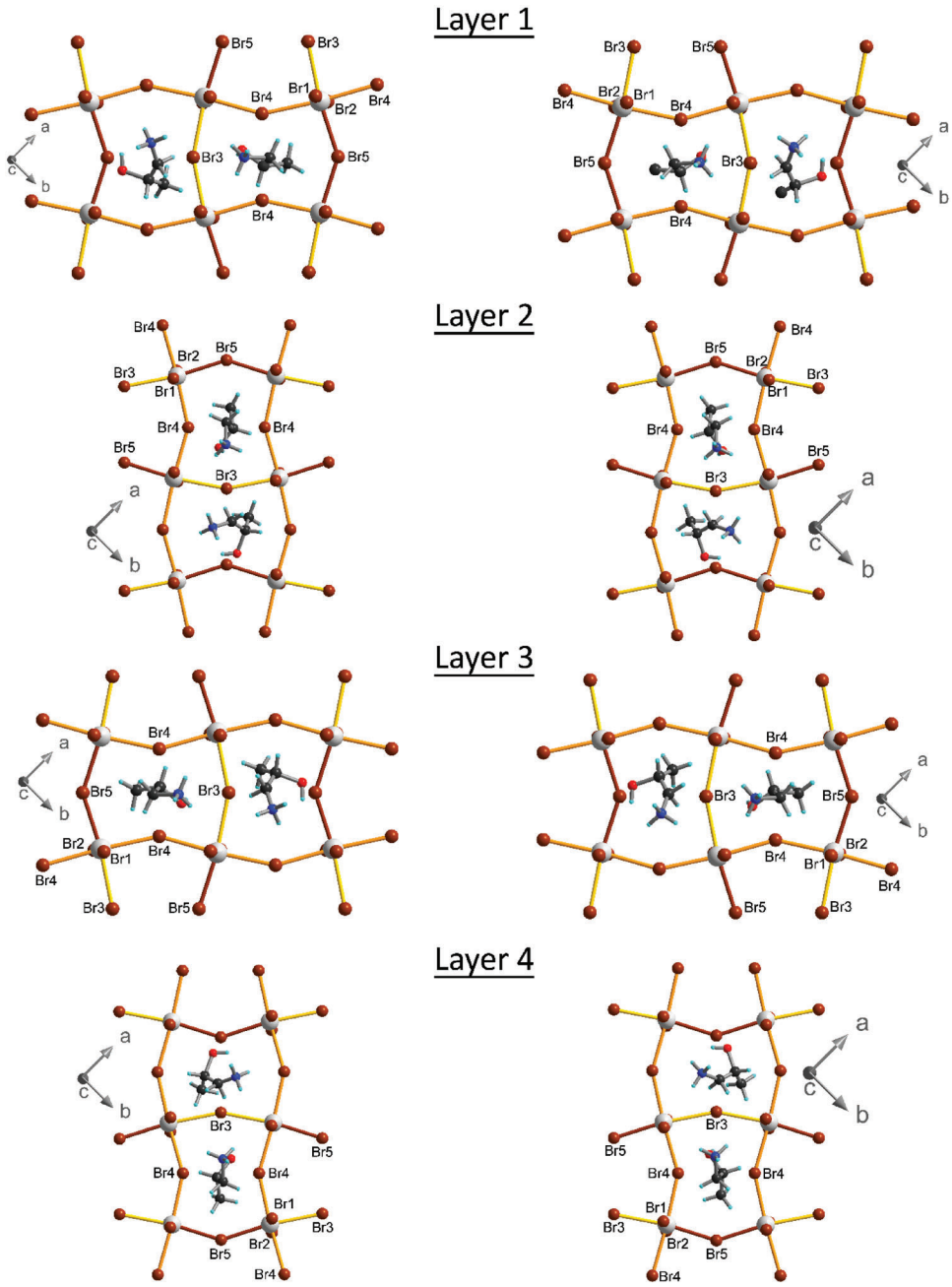

Figure 2. View of the four inorganic layers with closest cations in $(S\text{-HP1A})_2PbBr_4$ (left) and $(R\text{-HP1A})_2PbBr_4$ (right) with Br atom labels. Color code: C (black), H (cyan), N (blue), O (red), Br (brown), Pb (gray), longest Pb1–Br3 bond distances of 3.0763 Å (gold), intermediate Pb1–Br4 bond distances of 3.012–3.016 Å (orange), smallest Pb1–Br5 bond distances of 2.968 Å (brown).

runs along [1–10]. This incomplete effect leads to specific spin textures in which the spins are oriented in the stacking direction (Figure 4b and Figure S9, Supporting Information), the sign of the contribution changing depending on which half-plane is considered. When, taking into account the two types of layers simultaneously, we recover a splitting along both Γ→M and Γ→M', but the spin textures remain oriented solely along the stacking direction leading to rare spin textures where the signs of spin vary more rapidly. These computed textures differ notably from the ones speculated/hypothesized previously for nonpolar space groups. The original band structure can be understood as resulting from a superposition of alternating incomplete Rashba effects due to antiferroelectricity extending along the stacking axis with in-plane polarization (Figure S10, Supporting Information).

Owing to the band structure and associated spin textures, we envisaged these compounds as relevant materials for investigation of their spintronic properties. The phase purity of the polycrystalline samples was confirmed by powder X-ray diffraction (XRPD, Figure S11, Supporting Information). A dimethylformamide solution of each sample was used to prepare thin

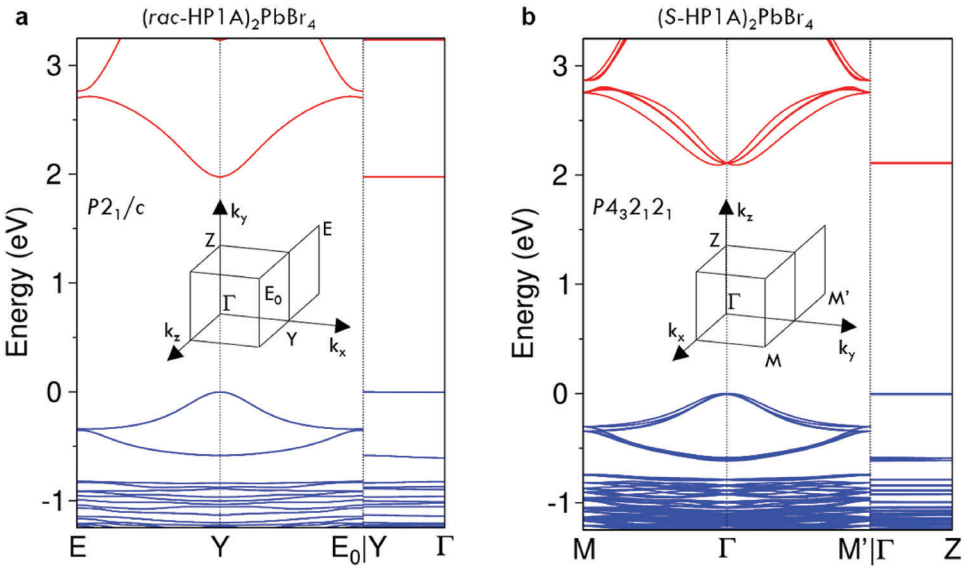

Figure 3. Density functional theory (DFT) computed band structure of (*rac*-HP1A)$_2$PbBr$_4$ (a) and (*S*-HP1A)$_2$PbBr$_4$ (b). Insets show the respective Brillouin zones. Both structures present features of two-dimensional (2D) like materials with strong dispersion within the perovskite plan, while flat bands are obtained along the stacking directions Y–Γ and Γ–Z. (*rac*-HP1A)$_2$PbBr$_4$ presents a direct band gap at Y, because of a splitting of bands away from the high-symmetry point, (*S*-HP1A)$_2$PbBr$_4$ has a slightly indirect band gap near Γ.

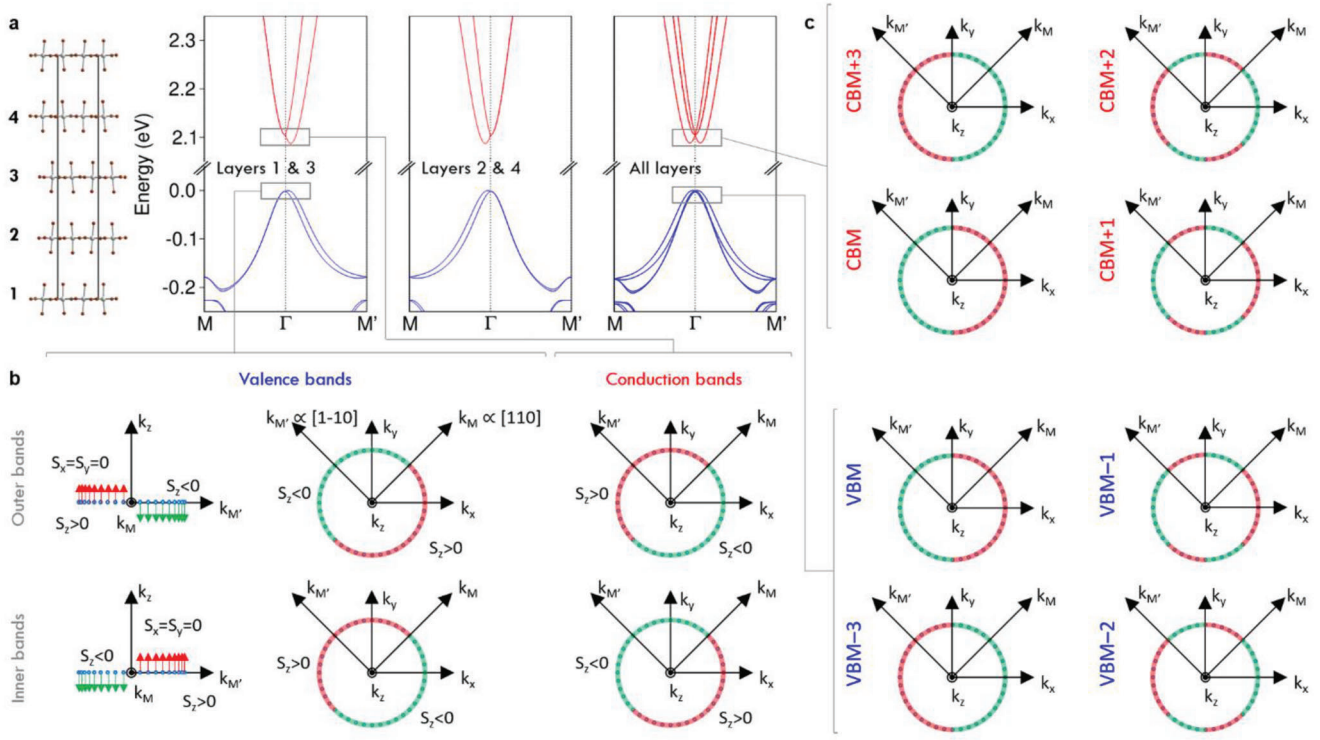

Figure 4. a) Density functional theory (DFT) computed band structure of (*S*-HP1A)$_2$PbBr$_4$ (with *S*-HP1A cations substituted by Cs ions) with only layers 1 and 3 (left), 2 and 4 (middle), or all layers (right). When only one set of layers is considered, an incomplete Rashba splitting is found with a splitting only in one direction of the plane, while the degeneracy is recovered along the polar axis of the layers. b) Schematic representation of the computed spin textures for the inner and outer bands at the valence and bottom edges of layers 1 and 3. In the case of an incomplete Rashba, the spins are aligned along the stacking direction with positive ($S_z > 0$, red arrows) contributions on half of the plane and negative ($S_z < 0$, green arrows) for the other half. c) Same for the complete structure with all layers.

films on FTO substrates by spin-coating. The films are highly oriented with the 2D layers parallel to the substrates as shown by the presence of only (00l) peaks in the diffraction patterns (Figure S12, Supporting Information). To confirm the chiroptical activity from the inorganic network, CD has been performed on the thin films. The exciton absorption shows a relatively broad peak with a maximum at 392 nm, typical of the $PbBr_4^{2-}$ inorganic network (**Figure 5**). Mirror-image CD spectra could be obtained in the vicinity of absorption maxima and show negative and positive Cotton effects for the *S* and *R* enantiomers,respectively. A second Cotton effect can be observed at higher energies, with a change of sign in the CD signal at around 315 nm. The g_{abs} factor was calculated by dividing the ellipticity with absorption of the films. *S* and *R* enantiomers present highest g_{abs} values of about -3.10^{-4} and $+3.10^{-4}$, respectively (Figure S13, Supporting Information).

The greater structural and optical stability of 2D lead–bromide HPs compared to their lead–iodide congeners was recently demonstrated.[22] To confirm this stability in $(S/R\text{-HP1A})_2PbBr_4$, spin-coated thin films were prepared and kept under light and 40–50% relative humidity atmosphere over a period of one month. Periodic XRPD and UV–Vis absorption measurements were collected during this time. XRPD diffraction patterns show thin films of $(S/R\text{-HP1A})_2PbBr_4$ remain highly crystalline, with a slight decrease of the first peaks relative intensities (<5%, see Figure S14, Supporting Information). UV–Vis absorption and CD spectra confirm the integrity of the chiroptical properties with a 10% loss of relative intensity at the maximum absorption wavelength over the entire period (Figure S15, Supporting Information). These subtle changes in both CD, absorption spectra, and XRPD indicate a slight modification of the film's morphology, but no sign of degradation (for example by appearance of $PbBr_2$ degradation product) was observed after 1 month under light and moisture conditions. These reliable (and yet nonoptimized) series of tests confirm the high potential of such materials for device construction and engineering.

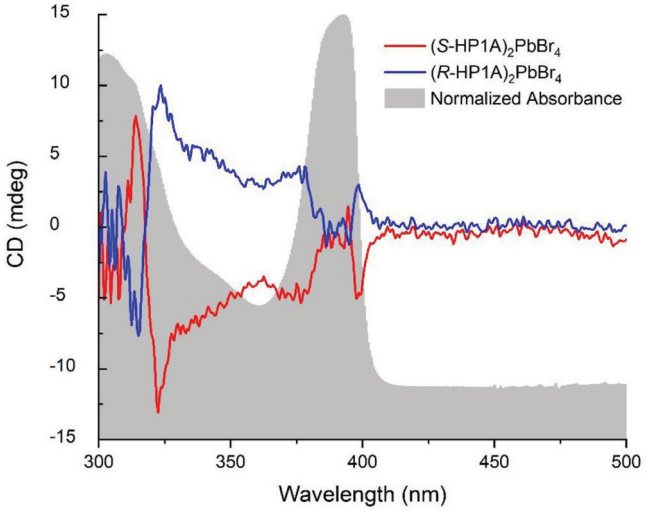

Figure 5. Circular dichroism (CD) and absorbance spectra of thin films of $(S\text{-HP1A})_2PbBr_4$ and $(R\text{-HP1A})_2PbBr_4$ recorded in the transmission mode.

The stability and chiral character of the inorganic network confirmed in $(S/R\text{-HP1A})_2PbBr_4$, the spin selectivity in electronic transport could be investigated. Recently, the team of Beard has reported the first CISS effect in 2D iodide-based chiral HPs and show similar behaviors for compounds based on lead[7] or tin,[8] with SP values as high as 86% and 94% respectively. Such measurements focus on out-of-plane conductivity (i.e., perpendicular to the 2D layers) and thus correspond to a spin-polarized charge transport in the tunneling regime. Up to now, this out-of-plane transport was associated to the presence of twofold symmetry ($P2_12_12_1$ space group in the previously studied compounds), however in $(S/R\text{-HP1A})_2PbBr_4$ it is now possible to highlight the impact of 4_1 screw axis in the SP ability of 2D HPs. In this purpose, magnetic conducting atomic force microscopy (mc-AFM) measurements were performed to examine the spin selectivity of the electron transfer through $(S/R\text{-HP1A})_2PbBr_4$ samples (**Figure 6**). To monitor electron transport, the spin coated samples were deposited on a FM Nickel, 100 nm thick substrate coated with a thin (10 nm) Au layer, which can be magnetized with the North magnetic pole pointing towards the layer (up) or away from the layer (down). In the present investigations, the nonmagnetic AFM tip was grounded and the potential on the conducting Au/Ni surface was changed. Current versus voltage (*I*–*V*) were performed on $(S/R\text{-HP1A})_2PbBr_4$ thin films for at least 50 individual measurements (Figures S16, Supporting Information). The corresponding average *I*–*V* curves clearly show two different onsets of the currents in the different magnetic field directions, each corresponding to different SP (Figure 6). The magnetic field that controls the spin selectivity of one enantiomer is opposite to that of the other enantiomer, which proves the role of chirality in spin selective investigations. Further, the variance in threshold voltage for the injection of two spins is an indication that no spin flipping occurs during electron transmission through $(S/R\text{-HP1A})_2PbBr_4$ thin films. Furthermore, the percentage of SP% is calculated using formula $SP\% = \frac{(I_{up} - I_{dn})}{(I_{up} + I_{dn})} \times 100$, where I_{up} and I_{dn} represent the current when the north pole of the magnetic field is directed upward or downward direction, respectively. As shown by the dependence of the SP on the applied voltage (Figure 6), calculated values of SP% are of the order of 40–45%.

At this step, one could try to relate these results with the two reported CISS measurements on related 2D chiral HPs. Despite the fact that the results obtained from such types of measurements can be strongly dependent on experimental setup and preparation conditions, the huge difference in SP% values between the present examples and the previously reported compounds of formula $(S/R\text{-MBA})_2PbI_4$ and $(S/R\text{-MBA})_2SnI_4$ suggests at first a possible spin-dephasing within the inorganic sublattice in $(S/R\text{-HP1A})_2PbBr_4$. Such behavior may be understood on the basis of composition and crystal structures. First, compared to our results, the 86% SP observed in thin films of $(S/R\text{-MBA})_2PbI_4$ excludes the predominant role of SOC from the metal ion (same in both compounds) for efficient CISS effect. Since the out-of-plane electron transport here involved is dominated by a tunneling process, one must look at the stacking of the layers in the 2D structure. For example, the X···X interlayer distance of 8.05 Å in $(S/R\text{-MBA})_2PbI_4$ and $(S/R\text{-MBA})_2SnI_4$ is much higher than in $(S/R\text{-HP1A})_2PbBr_4$ (6.52 Å, Figure S17, Supporting Information). This 20% reduction of interlayer distance in

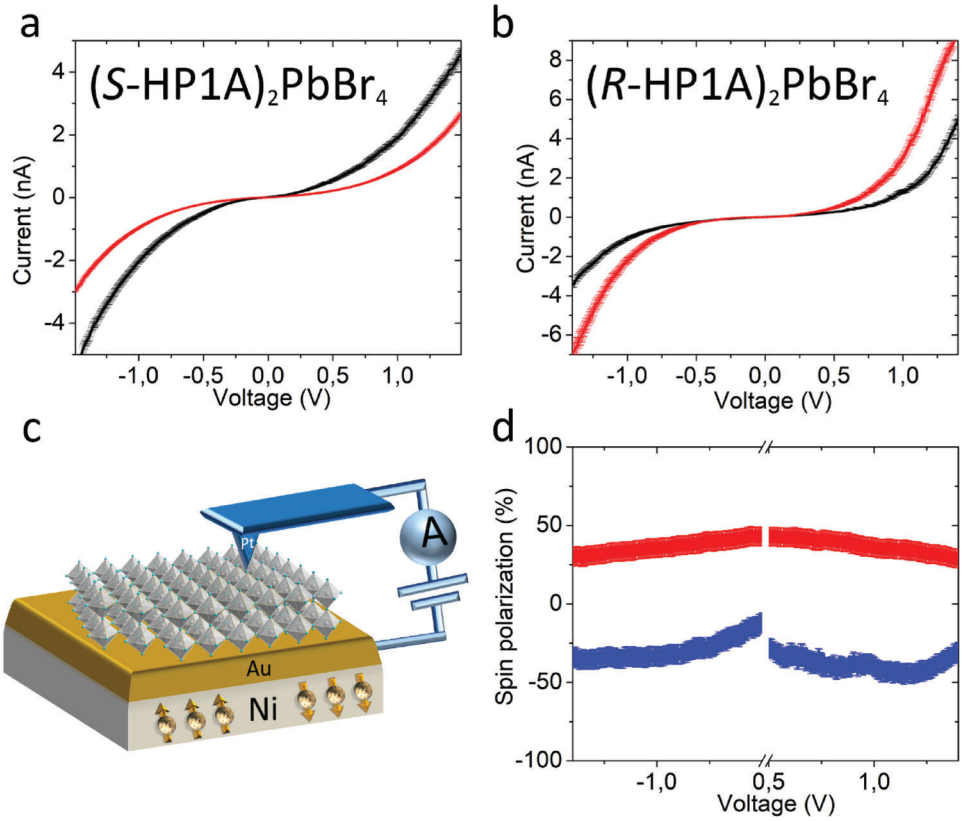

Figure 6. a,b) Room temperature magnetic conducting atomic force microscopy (mc-AFM) measurements for (*S*-HP1A)$_2$PbBr$_4$ and (*R*-HP1A)$_2$PbBr$_4$. c) Schematic representation of the experimental setup. d) Average values of spin polarization (SP) in (*S*-HP1A)$_2$PbBr$_4$ (red) and (*R*-HP1A)$_2$PbBr$_4$ (blue).

(*S*/*R*-HP1A)$_2$PbBr$_4$ may decrease the SP of the carriers. Indeed, in helical organic molecules such as DNA and oligopeptides, it was described that the increase of the pitch of the helix reduces more the transmission of the unfavored spin rather than the favored one, therefore the SP increases by increasing the tunneling barrier.[6] By analogy in chiral HPs, increasing the interlayer distance is also expected to improve the selectivity of the conduction electron's spin, thus contributing to the much higher SP observed in (*S*/*R*-MBA)$_2$PbI$_4$ and (*S*/*R*-MBA)$_2$SnI$_4$ than in (*S*/*R*-HP1A)$_2$PbBr$_4$.

On the other hand, both compounds present in-plane distortions of the 2D layers, with stronger distortions observed in (*S*/*R*-HP1A)$_2$PbBr$_4$ (Figure S18, Supporting Information) and almost any out-of-plane distortion. According to a previous study from Mitzi et al., a stronger in-plane distortion leads to a more effective spin-splitting.[15] However, this effect only considers individual 2D layers. A higher variation of polarity direction in (*S*/*R*-HP1A)$_2$PbBr$_4$ (due to the fourfold symmetry operations) compared to (*S*/*R*-MBA)$_2$PbI$_4$ and (*S*/*R*-MBA)$_2$SnI$_4$ (twofold symmetry, Figure S10 , Supporting Information), leading to the spin textures described earlier may produce a larger spin scattering of the charge carriers in the present compounds. An alternative explanation is based on the observation that the two types of chiral structures lead to different ordering of the spin textures (see Figure S19 , Supporting Information, for (*S*-MBA)$_2$PbI$_4$, Supporting Information) and therefore ordering of the spin densities of states along the stacking axis. According to Julliere's law, it is known that the vertical spin current and the tunnel magnetoresistance (MR), strongly depend on the spin densities on both side of a tunnel junction, opposite spin densities being unfavorable for large spin current.[23] The analogy between the tunnel MR concept and CISS effects in organic materials has already been used down to a single helical natural protein molecule.[24] Through all these considerations, it thus appears that SP is strongly affected by the crystallographic structure and its space symmetries as well as interlayer distances in this family of 2D hybrid organic/inorganic semiconductors. Future studies should help to independently evaluate the impact of both features.

Nevertheless, these iodide-free 2D materials represent an interesting alternative for the construction of chiro-spintronic devices with long-term stability. In this context, we have fabricated a spin-valve device with each enantiomorphic material using single FM electrode. Compared to mc-AFM measurements that revealed the spin-selective transport at single molecular level (thus avoiding the possibility of losing SP due to the presence of pinholes at the film surface), MR measurements in spin valves allow to measure the spin-filtering from a large area. The device was made with crossbar geometry and the measurement was done using four-probe configuration (**Figure 7**a). MR measurements in spin valves are performed from room temperature to cryogenic temperatures, as the MR signal sharply changes by increasing temperature.[25] MR is defined as MR (%) = $\frac{(R_B - R_{B=0})}{(R_{B=0})} \times 100$, where $R_{B=0}$ and R_B are the zero-field and infield resistances,

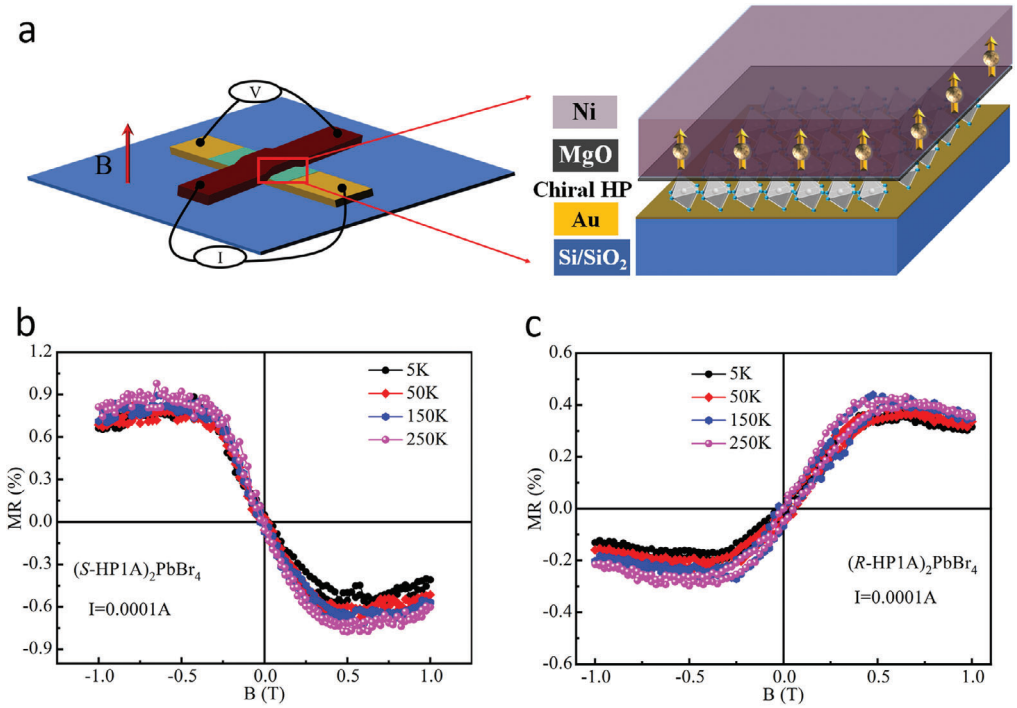

Figure 7. a) Schematic representation of the four-probe spin-valve device with bottom Au and top Ni as single FM electrode. MR responses for (*S*-HP1A)$_2$PbBr$_4$ b) and (*R*-HP1A)$_2$PbBr$_4$. c) The MR measurements were performed as a function of magnetic field (between -1T to +1T) at a constant current of 0.0001 A.

respectively. As a new strategy, we decided to measure MR of our chiro-spintronic device at different temperatures upon application of an out-of-plane magnetic field B, which is perpendicular to the 2D layers. The MR spectra of both helix of perovskites were collected by scanning from −1 to +1 T (Figure 7b,c). Differently from traditional spin-valve devices, here the signal is almost independent to the external temperature, with a slight and linear increase of the MR response when going from 5 to 250 K. This critical aspect further highlights the applicability of such chiro-spintronic devices over those based on FM materials. The spectra revealed the asymmetry in MR curve as a function of magnetic field, which is opposite between enantiomorphic materials, as a further demonstration of the CISS effect. The ΔMR (%) value, defined as ΔMR (%) = $|\text{MR (\%)}|_{-1T}$ + $|\text{MR (\%)}|_{+1T}$, is estimated at around 1.7% and 0.8% for (*S*-HP1A)$_2$PbBr$_4$ and (*R*-HP1A)$_2$PbBr$_4$, respectively. It should be noted that in MR measurements, all the electrons flowing through the device are collected, namely, electrons flowing through the chiral molecular layer and those ejected through pinholes or bare gold. Therefore, MR measurement method gives very small SP values compared to mc-AFM. Consequently, the large difference in MR(%) and ΔMR(%) between the two enantiomers might be due to the nonuniformity of the spin-coated thin films on bottom electrode. Finally, the decrease in MR at high field is probably due to the overshoots/undershoots in resistance with increase of magnetic field. These anomalies might due to the electron–electron interaction as previously observed in two-dimensional electron systems.[26,27]

3. Conclusion

A pair of enantiomorphic compounds (*S*-HP1A)$_2$PbBr$_4$ and (*R*-HP1A)$_2$PbBr$_4$ was obtained both as single crystals and highly crystalline thin films. The presence of fourfold screw axes in the crystal structures induces a peculiar arrangement of the 2D layers. The 90° rotation between neighboring layers results in a high variation of polarization direction around the stacking axis. Therefore, the band structure is made of alternating Rashba-like splittings of the layers, leading to rare spin textures at the top valence and bottom conduction bands. Such antiferroelectric array may be at the origin of a spin-scattering resulting in an incomplete spin selectivity of the conductions electrons as revealed by mc-AFM measurements, with SP% far from 100%. Still, a spin-valve device based on these materials could be prepared and evaluated. The results show that even an incomplete effect is efficient enough to drive a chiro-spintronic device such as spin valves. It also reveals the tremendous potential of 2D chiral HPs for controlling both charge and spin degrees of freedom in a new generation of devices based on chiral materials and powered by a tunneling process. Future works may demonstrate the processability of such materials in many different device architectures based on chiro-spintronics. At the same time, the preparation of more chiral HP materials is required in order to reach higher MR values for practical applications of spin-valve devices.

[CCDC 2267658–2267660 contain the supplementary crystallographic data for this paper. These data can be obtained free of charge from The Cambridge Crystallographic Data Centre via www.ccdc.cam.ac.uk/data_request/cif.]

Supporting Information

Supporting Information is available from the Wiley Online Library or from the author.

Acknowledgements

The work in France was supported by the CNRS and the University of Angers. A.K. and T.K.D. acknowledge the support by the ERC Synergy project CASTLE (proj. n. 101071533) funded by the Horizon Europe Program. J.E. acknowledges the financial support from the Institut Universitaire de France. The work at ISCR and Institut FOTON was performed with funding from the European Union's Horizon 2020 program, through a FET Open research and innovation action under the grant agreement No 899141 (PoLLoC). This work was granted access to the HPC resources of TGCC under the allocations 2022-A0130907682 made by GENCI. A.A. thanks Prof. Ron Naaman and Dr. Maurizio Mastropasqua Talamo for fruitful discussions.

Conflict of Interest

The authors declare no conflict of interest.

Data Availability Statement

The data that support the findings of this study are available from the corresponding author upon reasonable request.

Keywords

chiral perovskites, chiro-spintronics, CISS effect, Rashba-like splittings, spin valves

Received: June 15, 2023
Revised: July 29, 2023
Published online:

[1] R. Naaman, Y. Paltiel, D. H. Waldeck, *Nat. Rev. Chem.* **2019**, *3*, 250.
[2] F. Evers, A. Aharony, N. Bar-Gill, O. Entin-Wohlman, P. Hedegård, O. Hod, P. Jelinek, G. Kamieniarz, M. Lemeshko, K. Michaeli, V. Mujica, R. Naaman, Y. Paltiel, S. Refaely-Abramson, O. Tal, J. Thijssen, M. Thoss, J. M. van Ruitenbeek, L. Venkataraman, D. H. Waldeck, B. Yan, L. Kronik, *Adv. Mater.* **2022**, *34*, 2106629.
[3] H. Lu, Z. Valy Vardeny, M. C. Beard, *Nat. Rev. Chem.* **2022**, *6*, 470.
[4] P. S. Sercel, Z. Valy Vardeny, A. L. Efros, *Nanoscale* **2020**, *12*, 18067.
[5] Z. Xie, T. Z. Markus, S. R. Cohen, Z. Vager, R. Gutierrez, R. Naaman, *Nano Lett.* **2011**, *11*, 4652.
[6] V. Kiran, S. R. Cohen, R. Naaman, *J. Chem. Phys.* **2017**, *146*, 092302.
[7] H. Lu, J. Wang, C. Xiao, X. Pan, X. Chen, R. Brunecky, J. J. Berry, K. Zhu, M. C. Beard, Z. V. Vardeny, *Sci. Adv.* **2019**, *5*, eaay0571.
[8] H. Lu, C. Xiao, R. Song, T. Li, A. E. Maughan, A. Levin, R. Brunecky, J. J. Berry, D. B. Mitzi, V. Blum, M. C. Beard, *J. Am. Chem. Soc.* **2020**, *142*, 13030.
[9] Y. Lu, Q. Wang, R. Chen, L. Qiao, F. Zhou, X. Yang, D. Wang, H. Cao, W. He, F. Pan, Z. Yang, C. Song, *Adv. Funct. Mater.* **2021**, *31*, 2104605.
[10] C. Yuan, X. Li, S. Semin, Y. Feng, T. Rasing, J. Xu, *Nano Lett.* **2018**, *18*, 5411.
[11] J.-T. Lin, D.-G. Chen, L.-S. Yang, T.-C. Lin, Y.-H. Liu, Y.-C. Chao, P.-T. Chou, C.-W. Chiu, *Angew. Chem., Int. Ed.* **2021**, *60*, 21434.
[12] W. Wu, L. Li, D. Li, Y. Yao, Z. Xu, X. Liu, M. Hong, J. Luo, *Adv. Opt. Mater.* **2022**, *10*, 2102678.
[13] Y.-H. Kim, Y. Zhai, H. Lu, X. Pan, C. Xiao, E. Ashley Gaulding, S. P. Harvey, J. J. Berry, Z. Valy Vardeny, J. M. Luther, M. C. Beard, *Science* **2021**, *371*, 1129.
[14] A. Aziz, N. Aristidou, X. Bu, R. J. E. Westbrook, S. A. Haque, M. Saiful Islam, *Chem. Mater.* **2020**, *32*, 400.
[15] M. K. Jana, R. Song, Y. Xie, R. Zhao, P. C. Sercel, V. Blum, D. B. Mitzi, *Nat. Commun.* **2021**, *12*, 4982.
[16] G. Long, R. Sabatini, M. I. Saidaminov, G. Lakhwani, A. Rasmita, X. Liu, E. H. Sargent, W. Gao, *Nat. Rev. Mater.* **2020**, *5*, 423.
[17] M. Kepenekian, R. Robles, C. Katan, D. Sapori, L. Pedesseau, J. Even, *ACS Nano* **2015**, *9*, 11557.
[18] S. Krach, N. Forero-Correa, R.-I. Biega, S. E. Reyes-Lillo, L. Leppert, *J. Phys.: Condens. Matter* **2023**, *35*, 174001.
[19] M. K. Jana, R. Song, H. Liu, D. R. Khanal, S. M. Janke, R. Zhao, C. Liu, Z. Valy Vardeny, V. Blum, D. B. Mitzi, *Nat. Commun.* **2020**, *11*, 4699.
[20] Z.-G. Yu, *J. Phys. Chem. Lett.* **2020**, *11*, 8638.
[21] P. J. Huang, K. Taniguchi, M. Shigefuji, T. Kobayashi, M. Matsubara, T. Sasagawa, H. Sato, H. Miyasaka, *Adv. Mater.* **2021**, *33*, 2008611.
[22] E. S. Vasileiadou, I. Hadar, M. Kepenekian, J. Even, Q. Tu, C. D. Malliakas, D. Friedrich, I. Spanopoulos, J. M. Hoffman, V. P. Dravid, M. G. Kanatzidis, *Chem. Mater.* **2021**, *33*, 5085.
[23] M. Julliere, *Phys. Lett. A* **1975**, *54*, 225.
[24] Y. Matsuura, *Chem. Phys. Lett.* **2021**, *777*, 138741.
[25] J. P. Prieto-Ruiz, S. Gómez Miralles, H. Prima-García, A. López-Muñoz, A. Riminucci, P. Graziosi, M. Aeschlimann, M. Cinchetti, V. Alek Dediu, E. Coronado, *Adv. Mater.* **2019**, *31*, 1806817.
[26] I. Shlimak, V. Ginodman, A. B. Gerber, A. Milner, K.-J. Friedland, D. J. Paul, *EPL* **2005**, *69*, 997.
[27] E. M. Kendirlik, S. Sirt, S. B. Kalkan, W. Dietsche, W. Wegscheider, S. Ludwig, A. Siddiki, *Sci. Rep.* **2013**, *3*, 3133.